Catalytic properties of Al13TM4 complex intermetallics: influence of the transition metal and the surface orientation on butadiene hydrogenation

L. Piccolo, Corentin Chatelier, Marie-Cécile de Weerd, Franck Morfin, Julian Ledieu, Vincent Fournée, Peter Gille, Emilie Gaudry

Science and Technology of Advanced Materials

ISSN: 1468-6996 (Print) 1878-5514 (Online) Journal homepage: https://tandfonline.com/loi/tsta20

Catalytic properties of $Al_{13}TM_4$ complex intermetallics: influence of the transition metal and the surface orientation on butadiene hydrogenation

Laurent Piccolo, Corentin Chatelier, Marie-Cécile de Weerd, Franck Morfin, Julian Ledieu, Vincent Fournée, Peter Gille & Emilie Gaudry

To cite this article: Laurent Piccolo, Corentin Chatelier, Marie-Cécile de Weerd, Franck Morfin, Julian Ledieu, Vincent Fournée, Peter Gille & Emilie Gaudry (2019): Catalytic properties of $Al_{13}TM_4$ complex intermetallics: influence of the transition metal and the surface orientation on butadiene hydrogenation, Science and Technology of Advanced Materials

To link to this article: https://doi.org/10.1080/14686996.2019.1608792

Publisher: Taylor & Francis & The Author(s). Published by National Institute for Materials Science in partnership with Informa UK Limited, trading as Taylor & Francis Group.

Journal: *Science and Technology of Advanced Materials*

DOI: 10.1080/14686996.2019.1608792

Catalytic properties of $Al_{13}TM_4$ complex intermetallics: influence of the transition metal and the surface orientation on butadiene hydrogenation

Laurent Piccolo,[1*] Corentin Chatelier,[2,3] Marie-Cécile de Weerd,[2] Franck Morfin,[1] Julian Ledieu,[2] Vincent Fournée,[2] Peter Gille,[4] Emilie Gaudry[2*]

[1] *Univ Lyon, Université Claude Bernard - Lyon 1, CNRS, IRCELYON - UMR 5256, 2 Avenue Albert Einstein, F-69626 VILLEURBANNE CEDEX, France * laurent.piccolo@ircelyon.univ-lyon1.fr*
ORCID # 0000-0003-4095-0572

[2] *Université de Lorraine, CNRS, IJL, F-54000 Nancy, France * emilie.gaudry@univ-lorraine.fr*
ORCID # 0000-0001-6546-8323

[3] *Synchrotron SOLEIL, L'Orme des Merisiers, Saint-Aubin – BP 48, F-91192 GIF-sur-YVETTE CEDEX, France*

[4] *Department of Earth and Environmental Sciences, Crystallography Section, Ludwig-Maximilians-Universität München, Theresienstr. 41, D-80333 München, Germany*

Abstract

Complex intermetallic compounds such as transition metal (TM) aluminides are promising alternatives to expensive Pd-based catalysts, in particular for the semi-hydrogenation of alkynes or alkadienes. Here, we compare the gas-phase butadiene hydrogenation performances of *o*-$Al_{13}Co_4$(100), *m*-$Al_{13}Fe_4$(010) and *m*-$Al_{13}Ru_4$ (010) surfaces, whose bulk terminated structural models exhibit similar cluster-like arrangements. Moreover, the effect of the surface orientation is assessed through a comparison between *o*-$Al_{13}Co_4$(100) and *o*-$Al_{13}Co_4$(010). As a result, the following room-temperature activity order is determined: $Al_{13}Co_4$(100) << $Al_{13}Co_4$(010) < $Al_{13}Ru_4$ (010) < $Al_{13}Fe_4$(010). Moreover, $Al_{13}Co_4$(010) is found to be the most active surface at 110 °C, and even more selective to butene (100%) than previously investigated $Al_{13}Fe_4$(010). DFT calculations show that the activity and selectivity results can be rationalized through the determination of butadiene and butene adsorption energies; in contrast, hydrogen adsorption energies do not scale with the catalytic activities. Moreover, the calculation of projected densities of states provides an insight into the $Al_{13}TM_4$ surface electronic structure. Isolating the TM active centers within the Al matrix induces a narrowing of the TM d-band, which leads to the high catalytic performances of $Al_{13}TM_4$ compounds.

Keywords

Complex intermetallic compounds; $Al_{13}Fe_4$; $Al_{13}Co_4$; $Al_{13}Ru_4$; Heterogeneous catalysis; Hydrogenation; Butadiene; Density functional theory; Single-crystal surfaces

1. Introduction

The interest for intermetallic catalysts, *i.e.* compounds of at least two elements located left and around the Zintl line – vertical line between group 13 and group 14 [1] – in the periodic table, with a defined crystal structure and stoichiometry [2], has considerably increased in recent years [3,4]. The potential of these compounds lies in their stability, which is ensured by strong metal-metal bonds with an iono-covalent character for several of them, and the possibility to tune the catalytic activity and selectivity based on electronic, geometric and ordering effects [4]. Several examples can be found among noble metal-containing intermetallics such as Pd-Ga [5–10], Pd-In [10], Pd-Zn [11], and Pt-Sn [12], which are able to selectively catalyze alkyne (one triple C-C bond, as in acetylene) or alkadiene (two double C-C bonds, as in butadiene) hydrogenation. These reactions are of great industrial importance for, e.g., the processing of petrochemical products for polymer synthesis.

Pd-based catalysts are rare and costly but actually used in industrial processes. The addition of an inactive ancillary metal such as Ag, Au or Cu is known to improve the catalyst selectivity to partially hydrogenated products [2,13–15]. For the semi-hydrogenation of acetylene, low-cost alternatives to reference Pd-Ag in the form of Ni-Zn alloys were discovered through a theoretical approach based on the density functional theory [16]. However, under reaction conditions, such substitutional alloys may suffer from adsorption-induced surface segregation, accompanied with a decrease in selectivity [13,17,18].

The recent identification of transition-metal (TM) aluminides such as $Al_{13}Fe_4$, $Al_{13}Co_4$, and Al_5Co_2 as efficient catalysts for the semi-hydrogenation of acetylene or butadiene is a major breakthrough in the quest for noble metal-free catalysts [19–26]. Indeed, the chemical bonding network in these polar intermetallics, which are also quasicrystal approximants, may prevent any surface segregation process, ensuring the stability of the catalyst. The interest for polar intermetallic compounds, *i.e.* compounds with lower valence electron concentrations than those of the Zintl phases, but close to those of the Hume–Rothery phases [27], is not limited to catalysis. They have recently received extensive attention as attractive materials for a wide range of applications (permanent ferromagnets, magnetocalorics, shape-

memory alloys, superconductors, hydrogen storage materials, thermoelectrics). Several studies have compared the physical properties of $Al_{13}TM_4$ compounds along the series (TM = Co, Fe, Ru, Rh), but no drastic differences were highlighted, in line with similar vibrational and electronic properties in the series [23]. These approximants to decagonal quasicrystalline phases present specific crystal structures, described as a stacking of atomic planes perpendicular to the pseudo 10-fold direction - [100] for orthorhombic *o*-$Al_{13}Co_4$, [010] for monoclinic *m*-$Al_{13}Fe_4$ and *m*-$Al_{13}Ru_4$ - each plane presenting pentagonal atomic arrangements [28]. This leads to an anisotropy in the magnetic properties, as well as in charge and heat transport properties [29–31].

The complex structure of such polar intermetallics, involving mixed iono-covalent bonding, may also be of interest for heterogeneous catalysis. Owing also to the site isolation concept [5] already invoked to explain the high performance of $Al_{13}Fe_4$ towards the semi-hydrogenation of acetylene [19], the catalytic properties of $Al_{13}TM_4$ compounds are thus expected to be quite different from those of their pure TM counterparts. The surfaces of these materials can expose Al pentagons centered by the TMs, which are believed to be the catalytically active centers [32]. Besides, $Al_{13}Fe_4$ has been recently proposed as a template for substituting single Pt atoms at Fe sites [33].

Here, we focus on the comparison of the catalytic properties of $Al_{13}TM_4$ compounds (with TM = Fe, Co, Ru) for the gas-phase hydrogenation of butadiene, which an important petrochemical reaction for the purification of C4 cuts and the production of butenes before polymerization or alkylation [34–37]. This reaction is industrially performed on Pd-based catalysts, but it is also catalyzed by non-noble metals such as Fe, Co, and Ni, although with a much lower activity [38,39]. Our objective is to investigate the influence of the transition metal and the structure on the catalytic properties. Our rational approach combines experiments on oriented single-crystal surfaces, and theoretical calculations based on ideal infinite surfaces within periodic boundary conditions. The combination of experimental measurements with theoretical calculations is crucial here. Indeed, surface-science studies achieved under ultra-high vacuum (UHV) have already highlighted that the pseudo 10-fold surface structures of these compounds differ: a surface reconstruction is observed for $Al_{13}Ru_4$(010) [40], not for $Al_{13}Co_4$(100) and $Al_{13}Fe_4$(010) [41–43]. The surface structure and composition determined under UHV are also different between $Al_{13}Co_4$(100) and $Al_{13}Fe_4$(010). Nevertheless, catalytic properties are measured under gas pressure (typically a few millibars of reactants), which may imply different surface structures as compared to the UHV case. The consideration of a common surface model for all explored $Al_{13}TM_4$ pseudo 10-fold

surfaces ensures a sound comparison between the catalysts, and may help to conclude about the influence of geometric or electronic factors.

The paper is organized as follows. Materials, experimental and theoretical methods are described in Section 2. In section 3, the catalytic measurements are detailed, highlighting the superior performances of $Al_{13}Fe_4$(010) and $Al_{13}Co_4$(010) with respect to $Al_{13}Ru_4$(010) and $Al_{13}Co_4$(100). A rationalization of the catalytic properties of the three $Al_{13}TM_4$ pseudo 10-fold surfaces is then proposed, based on electronic structure calculations including the shapes of the density of states and the adsorption energies. Our results are finally discussed in Section 4.

2. Methods

2.1. Materials

Centimeter-size $Al_{13}TM_4$ (TM = Co, Fe, Ru) single crystals were grown from an Al-rich solution using the Czochralski method [44] and polished with diamond paste down to 0.25 µm grain size. For the investigation of the catalytic properties, samples with surfaces oriented perpendicular to the pseudo-10-fold axis were cut from the ingot: *o*-$Al_{13}Co_4$(100), *m*-$Al_{13}Fe_4$(010) and *m*-$Al_{13}Ru_4$(010). An additional sample, *o*-$Al_{13}Co_4$(010), was used to investigate the influence of the surface orientation on the catalytic performances. In the following, when *o* or *m* prefixes are not mentioned, the crystal structures correspond to those of the above four samples.

2.2. Experimental methods

2.2.1. Surface preparation

For each sample, the surface was cleaned by repeated cycles of Ar^+ sputtering (2 kV) for 15 min and annealing for 20 min under UHV (base pressure ~5×10^{-10} Torr). The annealing temperatures were approximately 550-650 °C and 800 °C for $Al_{13}Co_4$(100), 750 °C for $Al_{13}Fe_4$(010) [22], 550 °C and 800 °C for $Al_{13}Ru_4$(010), and 800 °C for $Al_{13}Co_4$(010). Figure 1 and Figure S1 (Supplementary Information) show the low-energy electron diffraction (LEED) patterns and Auger electron spectra (AES), respectively, of the clean annealed surfaces (for $Al_{13}Fe_4$(010) the reader may consult Ref. [22]). Figure S1 shows that no

contaminants such as C or O were detected by AES on any surface following the sputtering-annealing procedure.

In the case of $Al_{13}Co_4(100)$, the high-temperature (800 °C) annealing [41] led to a more disordered surface than the low-temperature one (650 °C), as shown by Figure 1. Conversely, the atomic order of $Al_{13}Ru_4(010)$ increased with the annealing temperature (lower background intensity), although the atomic structure of the surface remained essentially unchanged (Figure 1), consistently with the work of Ledieu *et al*. [40]. For both $Al_{13}Co_4(100)$ and $Al_{13}Ru_4(010)$, the two annealing temperatures led to similar near-surface compositions, as probed by AES. In the following, the results for $Al_{13}Co_4(100)$ and $Al_{13}Ru_4(010)$ relate to low-temperature and high-temperature annealing, respectively, unless explicitly mentioned. For $Al_{13}Fe_4(010)$ and $Al_{13}Co_4(010)$, only high-temperature annealing was performed and led to sharp LEED pattern (Figure 1). In the case of $Al_{13}Co_4(010)$, which had not been investigated so far, the main diffraction spots appear connected to each other through continuous and parallel lines. The corresponding surface structure is presently undetermined.

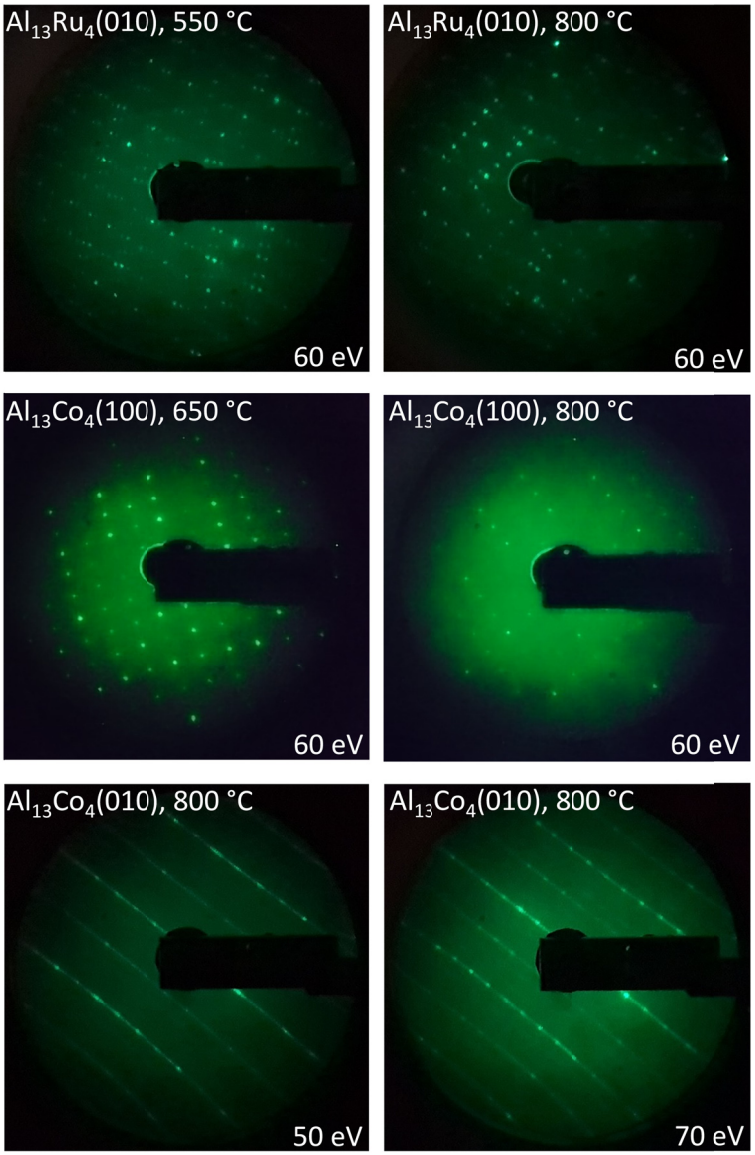

Figure 1. LEED patterns of clean annealed $Al_{13}Ru_4(010)$, $Al_{13}Co_4(100)$ and $Al_{13}Co_4(010)$ surfaces. The approximate annealing temperature (°C) and the primary energy (eV) are indicated.

2.2.2. Catalytic evaluation

The butadiene hydrogenation reaction was carried out in a dedicated static catalytic reaction cell (volume *ca*. 120 cm^3) coupled to a surface preparation/analysis (AES/LEED) setup [45]. In the cell, the sample was investigated either at room temperature (RT, 24 °C) or heated on the backside through a porthole using an infrared laser beam while the surface temperature was measured with an infrared pyrometer (surface emissivity set to 0.3). In a typical experiment, a mixture of butadiene (N26 purity),

hydrogen (N55) and argon (N56) was prepared in a separate chamber before its injection into the reactor. All the gases were purchased from Air Liquide. The standard initial conditions in the reactor cell were 0.5 mbar butadiene, 5 mbar H_2, and 0.5 mbar Ar (argon was used for internal calibration). At the end of the reaction run, the products were evacuated to secondary vacuum using a turbomolecular pump, and the reaction/evacuation cycle could be performed additional times.

During the reaction, the gases were continuously sampled through a leak valve and analyzed by a mass spectrometer (MS) evacuated by an oil diffusion pump capped with a LN_2 trap (base pressure 2×10^{-10} Torr, analysis pressure 2×10^{-8} Torr). The MS intensities for m/z = 2, 40, 54, 56, and 58 were recorded for hydrogen, argon, butadiene (C_4H_6), butenes (C_4H_8), and butane (C_4H_{10}), respectively. In some cases, on-line gas chromatography (GC) was employed in addition to MS for determining the full distribution of 1,3-butadiene hydrogenation products, *i.e.* the three butene isomers (1-butene, *trans*-2-butene and *cis*-2-butene) and butane, using an automatic gas sampling device connected to an Agilent 6850 GC-FID [45]. With an Agilent HP-AL/KCl column (50 m × 0.53 × 15 µm) kept at 80 °C, a chromatogram was recorded every 10 min.

2.3. Theoretical methods

2.3.1. Bulk and surface models

The *o*-$Al_{13}Co_4$ compound crystallizes in the *Pmn*2_1 space group [46], while *m*-$Al_{13}Fe_4$ and *m*-$Al_{13}Ru_4$ are monoclinic (C2/m space group) [47–49]. Their bulk structure (102 atoms per conventional cell, Figure 2) consists in a stacking of two types of planes perpendicular to the pseudo-10-fold direction ([010] for *m*-$Al_{13}Fe_4$ and *m*-$Al_{13}Ru_4$, [100] for *o*-$Al_{13}Co_4$). Alternative descriptions involve polyhedral atomic arrangements, such as the ones proposed by Henley [50], based on geometric considerations.

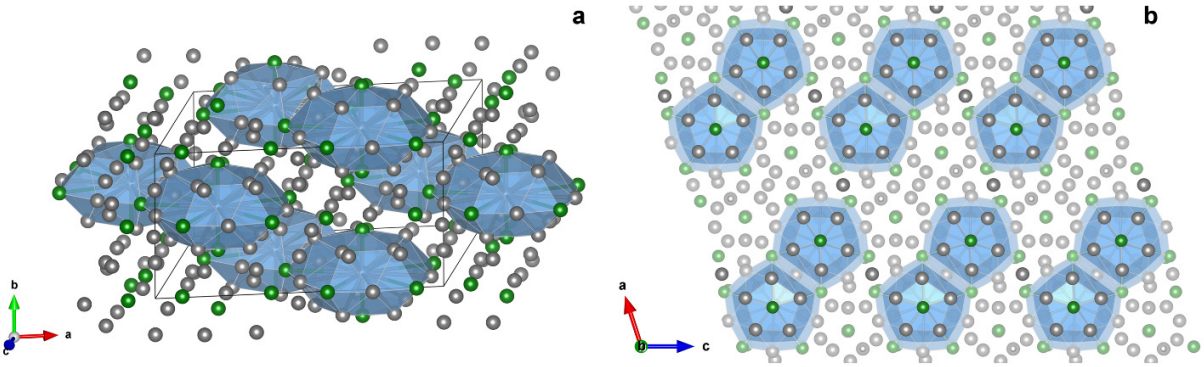

*Figure 2. (a) Bulk structure of $Al_{13}Ru_4$ as a stacking of Henley-type clusters (represented in blue). (b) Top view. Grey and green balls represent Al and Ru atoms, respectively. Shaded balls correspond to subsurface atoms. The crystal (a) and surface (b) directions are indicated by the unit vectors {***a***, ***b***, ***c***} and {***a***, ***c***}, respectively.*

The pseudo-10-fold surface models considered in this study are deduced from a cleavage keeping the cluster substructure intact at the surface (Fig. 2). Each protruding surface TM atom is surrounded by a pentagonal arrangement of Al atoms, leading to the isolation of TM atoms at the surface. Under UHV, such surface model has been experimentally observed in the case of *m*-$Al_{13}Fe_4$(010), but not for *o*-$Al_{13}Co_4$(100) and *m*-$Al_{13}Ru_4$(010) [40,42,51]. However, some operating conditions may stabilize the previous surface model (Gaudry *et al.*, in preparation), which has already been postulated to explain the catalytic activity of *o*-$Al_{13}Co_4$(100) towards the semi-hydrogenation of acetylene [32]. In addition, the consideration of the same surface model for all compounds should allow comparing the influence of the electronic factor (nature of the TM) on the adsorption properties.

2.3.2. Theoretical details

The theoretical ground state properties were deduced from calculations based on the density functional theory (DFT), using the plane wave Vienna *ab initio* simulation package (VASP) [52–55]. The interaction between the valence electrons and the ionic core was described using the projector-augmented wave (PAW) method [56,57] within the generalized gradient approximation (GGA-PBE) [58,59], considering the valences of the atoms to be $3s^2 3p^1$ (Al), $4s^1 3d^7$ (Fe), $4s^1 3d^8$ (Co),and $4p^6 5s^1 4d^7$ (Ru). The DFT-D3-BJ functional [60] was also used, since it is expected that the consideration of the van der Waals

interactions influences the absolute values of the adsorption energies. The cut-off energy and the k-point grid were set to 450 eV and 5×9×1 (or equivalent), respectively, within the Brillouin zone. Spin polarization was not taken into account since it was shown to be unnecessary for such Al-rich complex intermetallic compounds [61]**.** The structures were plotted using the VESTA software [62].

Bulk structures were relaxed till the Hellmann-Feynman forces were as low as 0.02 eV/Å. The resulting theoretical bulk parameters are found in good agreement with the experimental ones. As shown by Table S1, the relative differences are smaller than 1% (resp. 2%) for $Al_{13}Co_4$ and $Al_{13}Ru_4$ (resp. $Al_{13}Fe_4$). Adsorption studies were performed using surfaces modeled with 7-layer-thick symmetric slabs separated by void (thickness *ca.* 12Å). The positions of all the atoms in the slab were optimized, while the volume and the shape of the simulation cell were set. The adsorption energy for atomic hydrogen [E_{ads} (H)], and 1,3-butadiene or 1-butene [E_{ads} (but)] was calculated as the sum of the energies of the relaxed surface and the gas-phase molecule minus the energy of the adsorbate-surface system:

E_{ads} (H) = E(slab) + ½ E(H_2) – E(slab+H)

E_{ads} (but) = E(slab) + E(but) – E(slab+but)

where E(slab), E(H_2), E(but), E(slab+H) and E(slab+but) are the energies of the systems {slab}, {dihydrogen molecule}, {unsaturated hydrocarbon molecule}, {slab + atomic hydrogen} and {slab + unsaturated hydrocarbon molecule}, respectively.

With this definition, stable adsorption on the considered site corresponds to a positive value of E_{ads}.

Densities of states (DOS) of the d electrons $n_d(\varepsilon)$ were calculated for $Al_{13}TM_4$ compounds, as well as for the corresponding TMs (hcp Co, hcp Ru, bcc Fe). The d-band center is defined as:

$$dbc = \frac{\int_{-\infty}^{E_F+1\,eV} \varepsilon\, n_d(\varepsilon)\, d\varepsilon}{\int_{-\infty}^{E_F+1\,eV} n_d(\varepsilon)\, d\varepsilon} \quad (1)$$

where ε represents the energy and E_F the Fermi energy.

Projected DOS (pDOS) calculations were performed to investigate the molecule/surface interactions. The modifications of the molecular states following the adsorption process were evaluated from the comparison of the pDOS of the {molecule+surface} system, when the molecule is adsorbed at the surface and when the molecule is located far from the surface (distance larger than 10 Å).

3. Results

3.1. Experiments

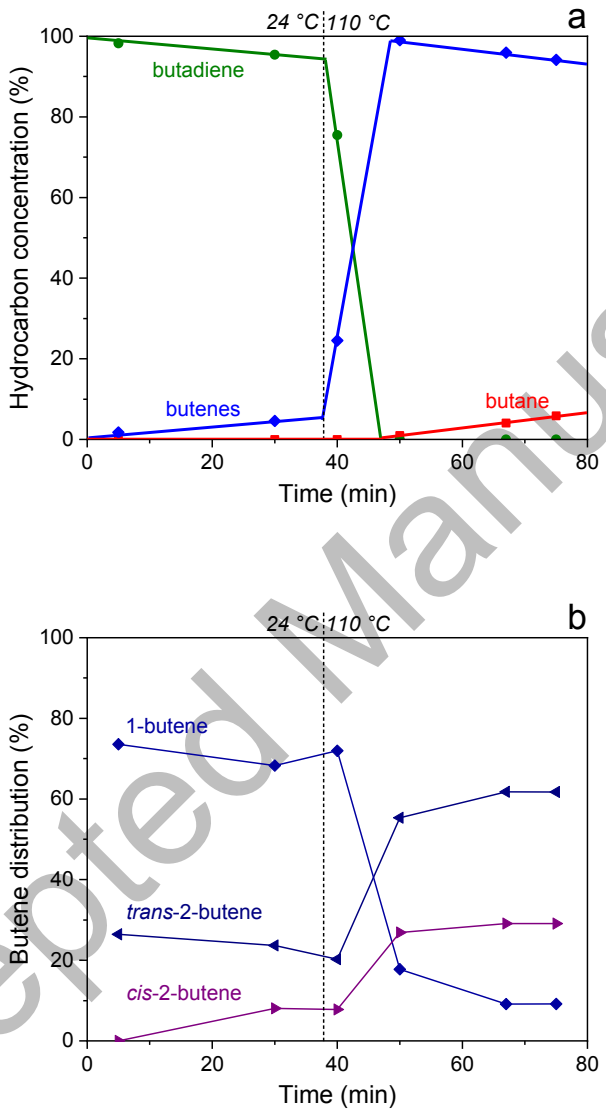

Figure 3. Hydrocarbon concentrations (a) and butene distribution (b) during butadiene hydrogenation over $Al_{13}Co_4$(010) at 24 °C, then 110 °C. The data points were obtained from GC analysis, whereas the lines in (a) were obtained from MS.

The clean annealed surfaces were exposed to a mixture of hydrogen (5 mbar) and butadiene (0.5 mbar) under batch conditions at RT and 110 °C. In all cases except that of $Al_{13}Fe_4$, the reaction kinetics was slow at RT, *i.e.* only a small fraction of butadiene was converted after *ca.* 30 min, so that the tests at 110 °C were generally performed during the same reaction run. Figure 3 shows the results of such an experiment for $Al_{13}Co_4$(010) (see also Fig. S2). Figures S3-S4 and S5-S6 show catalysis data for $Al_{13}Co_4$(100) and $Al_{13}Ru_4$(010), respectively. For detailed catalytic data concerning $Al_{13}Fe_4$(010), the reader may consult Ref. [22].

Figure 3a shows that the selectivity of $Al_{13}Co_4$(010) to butenes is 100%, both at RT and 110 °C, butane being formed only after complete butadiene conversion. The butene selectivity is also 100% for $Al_{13}Ru_4$(010) at any temperature (Fig. S5). For $Al_{13}Co_4$(100), it is 100% at RT at low conversion (Fig. S4) and superior to 95% at 110 °C (Fig. S3). The butene selectivity of $Al_{13}Fe_4$(010) is lower, but remains superior to 90% at any temperature. This lower selectivity correlates with the fact that $Al_{13}Fe_4$(010) is the only system, among the four $Al_{13}TM_4$ surfaces investigated, that exhibits a high activity for butene hydrogenation to butane (in the absence of butadiene). Butene hydrogenation over $Al_{13}Fe_4$(010) is even faster than butadiene hydrogenation in most conditions [22]. On the other surfaces, butene hydrogenation to butane is always slow (see Figure 3a for $Al_{13}Co_4$(010) and Fig. S5 for $Al_{13}Ru_4$(010), both at 110 °C).

In terms of initial butene distribution at RT (1-butene:*trans*-2-butene:*cis*-2-butene = 74:26:0%, Figure 3b), $Al_{13}Co_4$(010) behaves more like Pd(100) (73:24:3%) than $Al_{13}Fe_4$(010) (71:13:16%). For the latter system, an unusually low *trans*/*cis* 2-butene ratio, close to unity, was evidenced [22]. Conversely, for $Al_{13}Co_4$(010), *cis*-2-butene is not a primary product and its fraction remains lower than 10% throughout the reaction, as long as butadiene is present in the reactor, at both investigated temperatures. After butadiene conversion, the butenes distribution evolves towards a near-equilibrium value, 9:62:29%, through isomerization. As shown by Figure S4b, the butenes distribution for $Al_{13}Co_4$(100) throughout the reaction is similar to that for $Al_{13}Co_4$(010) (64:27:9% for the former vs. 68:24:8% for the latter, at t = 30 min and RT), although the initial 1-butene fraction is lower for $Al_{13}Co_4$(100) (64% vs 74%). In contrast, the surface orientation has a dramatic effect on the catalytic activity, $Al_{13}Co_4$(010) being much more active than $Al_{13}Co_4$(100) both at RT and 110 °C, as shown in Figure 4. Whereas in terms of activity at RT $Al_{13}Fe_4$(010) has no rival, $Al_{13}Co_4$(010) appears as the most active system at 110 °C while keeping a butene selectivity of 100% at any temperature. The faceting observed for $Al_{13}Co_4$(010) under UHV (Fig.

1), if retained under reaction conditions, may play an important role in its good catalytic performance. $Al_{13}Ru_4$(010) exhibits an activity intermediate between those of $Al_{13}Fe_4$(010) and $Al_{13}Co_4$(010).

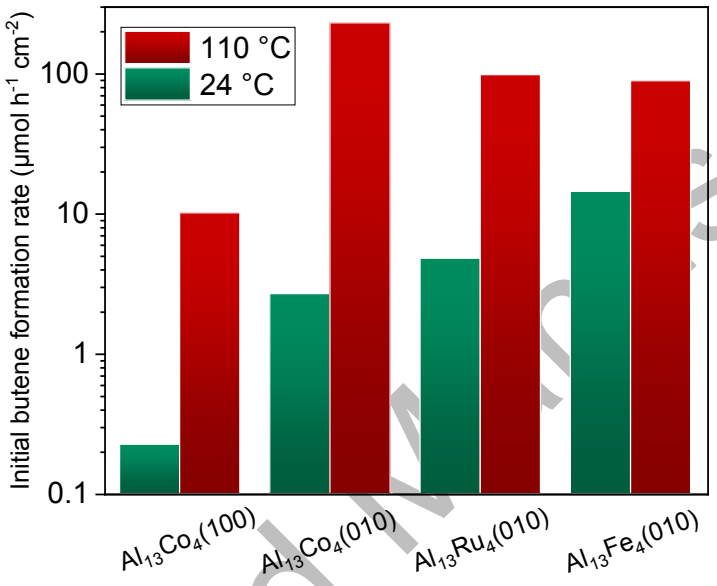

Figure 4. Comparison of initial butene-formation activities of $Al_{13}TM_4$ surfaces at RT and 110 °C.

In the case of $Al_{13}Ru_4$(010), similar experiments were carried out at RT for the Ar ion-sputtered surface, the surface annealed at *ca.* 550 °C, and the one annealed at *ca.* 800 °C. As a result, the activity of the sputtered surface is lower than that of the 550 °C-annealed surface, which is itself much lower than the activity of the (more structurally ordered) 800 °C-annealed surface (Fig. S6). Similarly, a lower activity of the sputtered sample was previously measured for $Al_{13}Fe_4$(010) [21], and is also observed here in the case of $Al_{13}Co_4$(010) (Fig. S2). Moreover, AES shows that the sputtered $Al_{13}TM_4$ surfaces are richer in TM than the annealed surfaces (Fig. S1). These results indicate that the structural and chemical orders, and correlatively the active center isolation, are beneficial to the hydrogenation activity of the Al-TM systems.

Our previous work on $Al_{13}Fe_4$(010) had shown that this surface is easily contaminated by oxygen-containing reactant impurities, most probably H_2O [21,22]. In the present work, when several subsequent reaction runs are performed on the same sample, the Co-containing surfaces show a loss of activity at any temperature (Figs. S2, S3), whereas $Al_{13}Ru_4$(010) deactivates at RT (Figs. S6) but not at 110 °C (Fig. S5). Both $Al_{13}Co_4$(100) and $Al_{13}Co_4$(010) contain, after reaction, not only oxygen but also traces of carbon, while $Al_{13}Ru_4$(010) contains only a small amount of oxygen (Fig. S1). The higher resistance of $Al_{13}Ru_4$(010) is tentatively ascribed to the presence of the noble metal (Ru) instead of Co or Fe.

3.2. Calculations

For $Al_{13}Co_4$(100), a previous study suggested favorable sites for the adsorption of atomic hydrogen, acetylene (C_2H_2) and ethylene (C_2H_4) *[32]*. Based on these results, only one type of site per adsorbate has been considered here for the pseudo 10-fold surface of $Al_{13}TM_4$ compounds: a bridge Al-TM site for atomic hydrogen, di-π adsorption of 1,3-butadiene (C_4H_6) on neighboring Al and TM atoms, and π adsorption of 1-butene (C_4H_8) on a TM atom. The corresponding geometries and adsorption energies (E_{ads}) are reported in Table 1.

Table 1. Adsorption configurations and energies (eV). The pictures were plotted using the $Al_{13}Ru_4$ model. Color code: Al=grey; Ru = green; C = red; H = black. Prefixes o and m relate to orthorhombic and monoclinic structures, respectively. PBE and D3 correspond to PBE and DFT-D3-BJ calculations, respectively.

		1,3-Butadiene	1-Butene	Hydrogen
		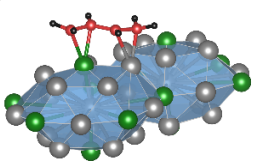	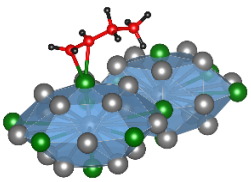	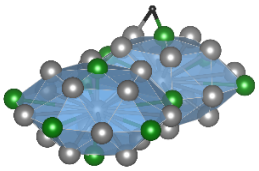
o-$Al_{13}Co_4$(100)	PBE	1.06	0.62	0.18
	D3	1.59	1.13	0.24
m-$Al_{13}Fe_4$(010)	PBE	1.30	0.91	0.39

	D3	1.80	1.38	0.41
m-$Al_{13}Ru_4$(010)	PBE	1.16	0.77	0.39
	D3	1.67	1.24	0.49

For atomic hydrogen adsorption, our result for $Al_{13}Co_4$(100) (E_{ads}^{PBE} = 0.18 eV) is in good agreement with the value reported in Ref. [32] (E_{ads}^{PBE} = 0.21 eV), and shows that atomic hydrogen is much less strongly bonded to $Al_{13}Co_4$(100) surface than to Co(0001) (E_{ads}^{PBE} = 0.48 eV [63]). On $Al_{13}Fe_4$(010) and $Al_{13}Ru_4$(010), considering the same type of Al-TM site, atomic hydrogen is bonded slightly stronger (E_{ads}^{PBE} = 0.39 eV). Again, these adsorption energies are lower than those calculated for Fe(110) (E_{ads}^{PBE} = 0.54 eV) and Ru(0001) (E_{ads}^{PBE} = 0.55 eV) [64,65]. These trends are also valid within the DFT-D3-BJ approach. The charge density deformation, defined as the charge density difference between the adsorbate-surface system and the sum of the charge densities for the relaxed slab and the adsorbate, plotted in Figure 5 for H/$Al_{13}Ru_4$(010), suggests a metal-H bond with an iono-covalent character. This is also consistent with the fact that H adsorption energies do not scale with the Bader charges held by TM atoms of the TM-Al-TM molecular group in the bulk (-3.83*e* for $Al_{13}Fe_4$, -4.08*e* for $Al_{13}Co_4$, and -4.32*e* for $Al_{13}Ru_4$).

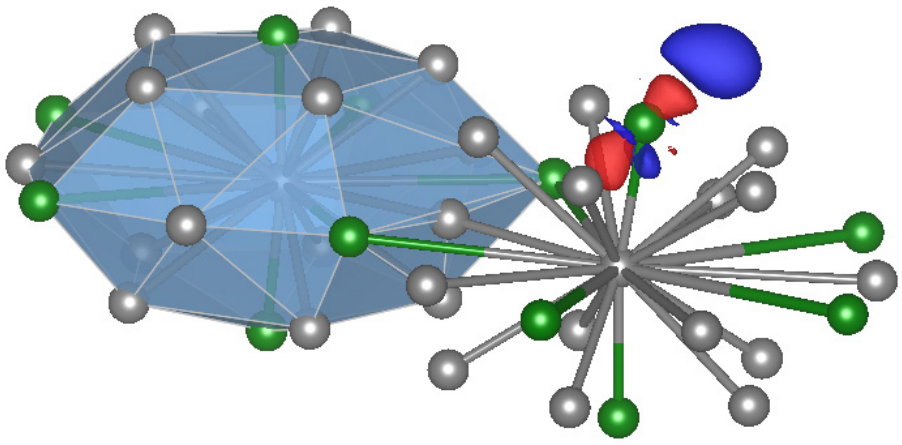

Figure 5. *Charge deformation following atomic hydrogen adsorption, highlighting the TM-H interaction (isodensity 0.007 Å^{-3}, plotted for H on $Al_{13}Ru_4$(010); the influence of the neighboring Al atom is not visible for this isodensity value). Charge accumulation and depletion are plotted in blue and red, respectively. The H atom is located inside the big blue distribution.*

On the pseudo-10-fold surfaces, the adsorption energy of butadfiene adsorbed in a di-π configuration increases from 1.06 eV (*o*-$Al_{13}Co_4$) to 1.16 eV (*m*-$Al_{13}Ru_4$) and 1.30 eV (*m*-$Al_{13}Fe_4$) within the PBE scheme (Table 1). The trends are similar when considering the van der Waals interactions, with E_{ads}(butadiene) increases from 1.59 eV (*o*-$Al_{13}Co_4$) to 1.67 eV (*m*-$Al_{13}Ru_4$) and 1.80 eV (*m*-$Al_{13}Fe_4$). The adsorption energies of 1-butene on the same surfaces are significantly lower, and the difference between E_{ads}(butadiene) and E_{ads}(butene) is almost constant (0.39-0.46 eV), regardless of the used functional.

Within the d-band model of Nørskov and coworkers, the d-band position and the d-band width were shown to be key parameters for rationalizing the adsorption properties of transition-metal surfaces [66,67]. This model was further developed to include the influence of the shape of the electron DOS [68]. To illustrate the role played by the TM atom isolation within the Al matrix, and in turn the electronic structure on the adsorption properties, we first compare the $Al_{13}Ru_4$(010) surface and the (low-energy) Ru(0001) surface, for which the adsorption energies of C_4H_6 are calculated to be 1.16 eV (Table 1) and 1.71 eV, respectively. On Ru(0001), only one adsorption site and configuration have been considered for C_4H_6, as shown in Figure S7.

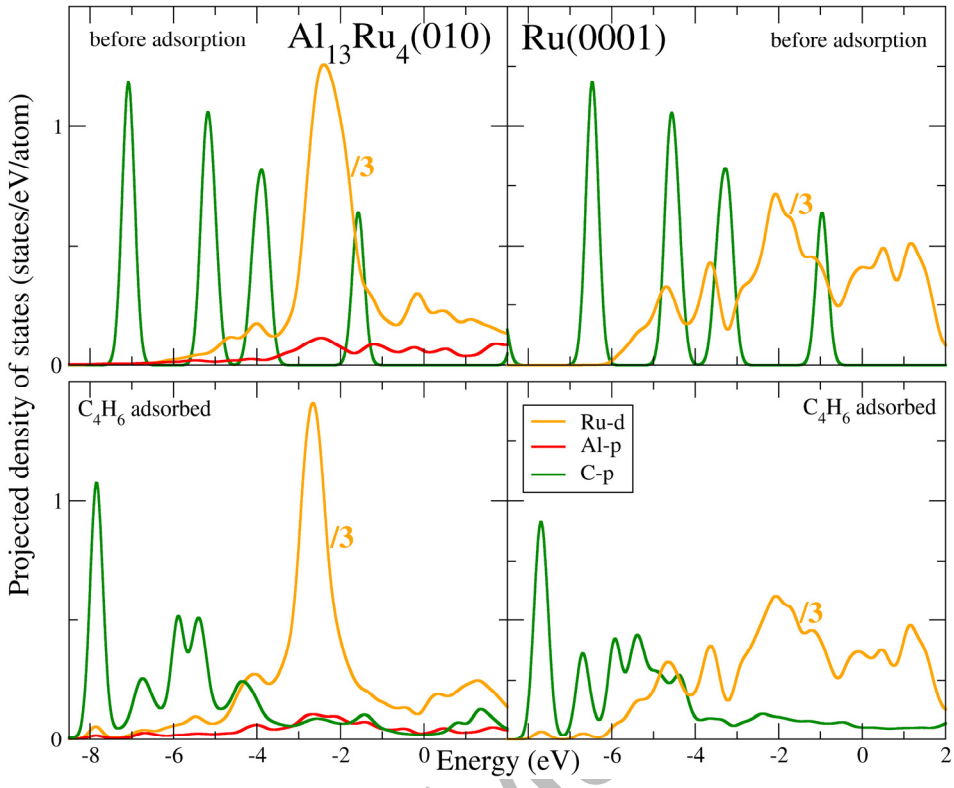

Figure 6. Projected density of states (pDOS): average C-p contribution of carbon atoms (butadiene, in green); Al-p (red) and Ru-d (orange) contributions of the closest Al and Ru atoms protruding at the surface and involved in the adsorption for $Al_{13}Ru_4$(010); Ru-d (orange) contribution of surface Ru atoms involved in the adsorption for Ru(0001). The Fermi energy was set to 0 eV.

The average contribution of the C-p orbital states in the butadiene molecule, as well as the Ru-d states involved in the adsorption, are represented in Figure 6. For Ru(0001), the contribution of Ru-d to the DOS is expanded on a much larger energy range (from the Fermi energy E_F up to binding energies of 6-8 eV) than for $Al_{13}Ru_4$(010), for which it is mostly localized around 2-3 eV. For Ru(0001), the contribution of Ru-d to the DOS is rather uniform on a large energy range (up to binding energies of 6 eV), while the Ru-d states are mostly localized around 2-3 eV for $Al_{13}Ru_4$(010). In both cases, the shapes and positions of the molecular states before adsorption (energies around -6.5 eV, -4.5 eV, -3.4 eV, and -1.0 eV) are modified upon adsorption, and new electronic states can be seen for E ≥ -8 eV, including states at the Fermi level arising from spd hybridization between the molecular and the surface states. In addition, a shift of the higher binding C-p state, located around -6.5 eV before adsorption and around -7.7 eV after

adsorption, is visible for the Ru(0001) and $Al_{13}Ru_4$(010) surfaces, consistent with electron transfer from the substrate to butadiene.

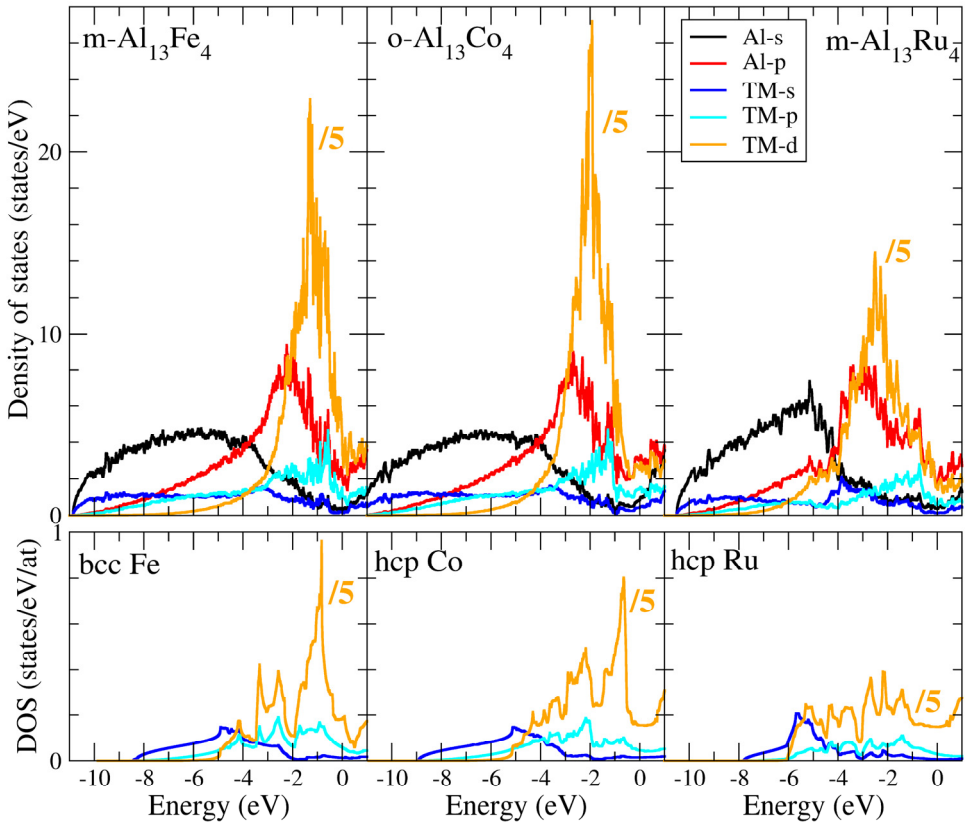

Figure 7. Contributions of s-, p-, and d-states to the density of states (DOS) for bulk $Al_{13}TM_4$ and TM. The Fermi energy corresponds to 0 eV.

To further look for a possible relationship between the d-band center position with respect to the Fermi energy (ΔE_{dbc}) and the catalytic performances, the bulk electronic structures of $Al_{13}Ru_4$, $Al_{13}Fe_4$ and $Al_{13}Co_4$ are compared in Figure 7. The DOSs of $Al_{13}Fe_4$ and $Al_{13}Co_4$ are similar, with a free electron-like shape at low energy, and a strong maximum at higher energy caused by localized and weakly dispersive TM-d states. These DOSs considerably differ from those of the pure metals (bottom graphs in Fig. 7), which exhibit a much more spread d-band, attributed to TM-TM hybridization. The latter is almost absent for $Al_{13}TM_4$ compounds, owing to the rather large nearest-neighbor TM-TM distance.

The stronger adsorption of butadiene on $Al_{13}Fe_4$(010) than on $Al_{13}Co_4$(100) (Table 1), classically attributed to a decreased filling of the adsorbate-metal antibonding states [69], is indeed in agreement with the lower-energy d-band center in the former case (ΔE_{dbc} ($Al_{13}Fe_4$) = 1.41 eV, ΔE_{dbc} ($Al_{13}Co_4$) = 1.97 eV).

However, the previous scheme is not consistent with the results found for $Al_{13}Ru_4$(010) (E_{ads} = 1.15 eV, ΔE_{dbc} = 2.48 eV), indicating that other parameters, such as the d-band width and shape, likely play a role.

4. Discussion

The comparison of butadiene-hydrogenation activities of $Al_{13}TM_4$ surfaces (Fig. 4) reveals a variety of behaviors, from the poor activity of $Al_{13}Co_4$(100) at any temperature to the high activities of $Al_{13}Fe_4$(010) at RT and $Al_{13}Co_4$(010) at 110 °C; $Al_{13}Ru_4$(010) shows intermediate activity, but superior stability. This implies that (i) for the pseudo 10-fold surfaces, Fe is the most active center; (ii) depending on the surface orientation, Co acts as a highly [(010)] or poorly [(100)] active center. If the $Al_{13}Co_4$(100) surface actually present in catalytic conditions has the same structure as under UHV, *i.e.* a bulk-terminated Al-rich termination without protruding Co atoms, it is indeed expected to be poorly active. However, since on the one hand the exact surface structure of $Al_{13}Co_4$(010) under UHV is unknown, and on the other hand any of the systems may reconstruct under reaction conditions, choice has been made to compare the electronic structures of unreconstructed, cluster-terminated pseudo 10-fold surfaces through DFT calculations. This has allowed us to focus, for a given atomic structure, on the effect of the TM nature (Ru, Co, Fe) and isolation (for Ru only) in an Al matrix on its surface electronic structure and corresponding bonding to the relevant adsorbates. As a result, site isolation is seen to considerably narrow the Ru d-band (Fig. 6), which leads to an adsorption energy reduced by 1/3. From the comparison of the bulk electronic structures of TM and $Al_{13}TM_4$ systems (Fig. 7), we have seen that TM isolation in the $Al_{13}TM_4$ structure proceeds similarly for the three TMs, *i.e.* by a narrowing of the d-band. Remarkably, the situation is here quite different from the one described in Ref. [70], where the stronger adsorption on the Ag-Cu "single-atom alloy" dilute in Cu, with respect to pure Cu, is attributed to the narrower d-band of the alloy as compared to pure Cu.

Butadiene/butene adsorption energies (Table 1) follow the same order as hydrogenation activities: $Al_{13}Fe_4$ > $Al_{13}Ru_4$ > $Al_{13}Co_4$. Hence, in this (low) adsorption energy range (1.1-1.3 eV for butadiene within PBE), the hydrocarbon adsorption energy can be considered as a semi-quantitative descriptor of the hydrogenation activity. On the pure metals, the much higher adsorption energies of the hydrocarbons may be detrimental to hydrogenation rates, as suggested by the lower activities of the TM-rich sputtered surfaces (SI). Moreover, the higher adsorption energy of butadiene with respect to butene is consistent

with a preference for butadiene adsorption and subsequent hydrogenation, *i.e.* to a high (near 100%) selectivity to butene [13,71]. In the sole case of $Al_{13}Fe_4$ butene appears sufficiently adsorbed to be (fastly) hydrogenated [22], whereas butene hydrogenation on the other $Al_{13}TM_4$ surfaces is very slow at any temperature (Section 3.1). The high butene-hydrogenation activity of $Al_{13}Fe_4$(010) is consistent with a selectivity to butene slightly lower than 100% in most butadiene-hydrogenation conditions.

In addition, the butenes distribution, and more specifically the *trans*/*cis* 2-butene ratio, is different between $Al_{13}Co_4$ (close to 3 for both orientations, and even much higher at the beginning of the reaction) and $Al_{13}Fe_4$ one (close to 1). Moyes *et al.* studied a number of TMs for butadiene hydrogenation and suggested that the electronic state of surface metal atoms would be the dominant factor driving the products distribution [39]. A high *trans*/*cis* 2-butene ratio was explained by the stabilization of π-allylic half-hydrogenated states which favored a selective pathway (as previously discussed for $Al_{13}Fe_4$(010) [22]) whereas πσ-adsorbed states favored *anti*/*syn* interconversion of the half-hydrogenated species and a more dispersed products distribution. Intermediate adsorbed species are not considered in the present work but a possible difference in the reaction pathways is consistent with the observed disparity in the apparent activation energy of the reaction over $Al_{13}TM_4$ compounds, *i.e.* $Al_{13}Co_4$(010) is the least active surface at RT but the most active one at 110 °C (Fig. 4).

As far as hydrogen adsorption is concerned, the adsorption energies for the $Al_{13}TM_4$ surfaces do not scale with the butadiene-hydrogenation activities (Table 1). However, the very low adsorption energy of H on $Al_{13}Co_4$(100) (E_{ads} < 0.2 eV) may contribute to the low hydrogenation activity of this surface.

In the future, a more quantitative theoretical description of the catalytic properties will have to include the effects of adsorbate coverage, thermodynamic conditions (pressure, temperature) and kinetics (reaction pathways including activation barriers).

5. Conclusions

On the basis of catalytic tests and DFT calculations, this work has allowed us to evidence trends in the electronic structures, adsorption properties and catalytic performances of the $Al_{13}TM_4$ intermetallic series. TM site isolation in the complex $Al_{13}TM_4$ structure induces a narrowing of the d-band and a decrease of the butadiene adsorption energy, leading to an enhanced hydrogenation activity. While $Al_{13}Fe_4$(010) is the most active model catalyst at room temperature, $Al_{13}Co_4$(010) is revealed as the most

active one at higher temperature (110 °C), while remaining 100% selective to butenes unlike $Al_{13}Fe_4$(010). In-depth investigations of $Al_{13}Co_4$(010) are needed to determine its structure and enable comparative DFT calculations. Moreover, a comprehensive understanding of the catalytic properties of these intermetallic surfaces requires *in situ* characterization (e.g. surface X-ray diffraction) to identify the actual working surface under gas-pressure conditions.

Acknowledgements

EG thanks Dr. David Loffreda for fruitful discussions. EG acknowledges financial support through the COMETE project (COnception in silico de Matériaux pour l'EnvironnemenT et l'Energie) funded by the "Région Lorraine". The work in Nancy was supported by the European Integrated Center for the Development of New Metallic Alloys and Compounds. High Performance Computing resources were provided by GENCI under the allocation 99642, as well as the EXPLOR center hosted by the Université de Lorraine (allocation 2017M4XXX0108).

References

[1] Meyer G, Naumann D and Wesemann L 2002 *Inorganic Chemistry Highlights* (Wiley)

[2] Vignola E, Steinmann S N, Vandegehuchte B D, Curulla D and Sautet P 2016 C_2H_2-Induced Surface Restructuring of Pd–Ag Catalysts: Insights from Theoretical Modeling *J. Phys. Chem. C* **120** 26320–7

[3] Armbrüster M, Schlögl R and Grin Y 2014 Intermetallic compounds in heterogeneous catalysis—a quickly developing field *Sci. Technol. Adv. Mater.* **15** 034803

[4] Furukawa S and Komatsu T 2017 Intermetallic Compounds: Promising Inorganic Materials for Well-Structured and Electronically Modified Reaction Environments for Efficient Catalysis *ACS Catal.* **7** 735–65

[5] Kovnir K, Armbrüster M, Teschner D, Venkov T V, Jentoft F C, Knop-Gericke A, Grin Y and Schlögl R 2007 A new approach to well-defined, stable and site-isolated catalysts *Sci. Technol. Adv. Mater.* **8** 420–7

[6] Osswald J, Giedigkeit R, Jentoft R E, Armbrüster M, Girgsdies F, Kovnir K, Ressler T, Grin Y and Schlögl R 2008 Palladium–gallium intermetallic compounds for the selective hydrogenation of acetylene: Part I: Preparation and structural investigation under reaction conditions *J. Catal.* **258** 210–8

[7] Osswald J, Kovnir K, Armbrüster M, Giedigkeit R, Jentoft R E, Wild U, Grin Y and Schlögl R 2008 Palladium–gallium intermetallic compounds for the selective hydrogenation of acetylene: Part II: Surface characterization and catalytic performance *J. Catal.* **258** 219–27

[8] Kovnir K, Osswald J, Armbrüster M, Teschner D, Weinberg G, Wild U, Knop-Gericke A, Ressler T, Grin Y and Schlögl R 2009 Etching of the intermetallic compounds PdGa and Pd_3Ga_7: An effective way to increase catalytic activity? *J. Catal.* **264** 93–103

[9] Armbrüster M, Kovnir K, Behrens M, Teschner D, Grin Y and Schlögl R 2010 Pd−Ga Intermetallic Compounds as Highly Selective Semihydrogenation Catalysts *J. Am. Chem. Soc.* **132** 14745–7

[10] Luo Y, Alarcón Villaseca S, Friedrich M, Teschner D, Knop-Gericke A and Armbrüster M 2016 Addressing electronic effects in the semi-hydrogenation of ethyne by InPd2 and intermetallic Ga–Pd compounds *J. Catal.* **338** 265–72

[11] Zhou H, Yang X, Li L, Liu X, Huang Y, Pan X, Wang A, Li J and Zhang T 2016 PdZn Intermetallic Nanostructure with Pd–Zn–Pd Ensembles for Highly Active and Chemoselective Semi-Hydrogenation of Acetylene *ACS Catal.* **6** 1054–61

[12] Jugnet Y, Sedrati R and Bertolini J-C 2005 Selective hydrogenation of 1,3-butadiene on $Pt_3Sn(111)$ alloys: comparison to Pt(111) *J. Catal.* **229** 252–8

[13] Piccolo L, Piednoir A and Bertolini J-C 2005 Pd–Au single-crystal surfaces: Segregation properties and catalytic activity in the selective hydrogenation of 1,3-butadiene *Surf. Sci.* **592** 169–81

[14] Hugon A, Delannoy L, Krafft J-M and Louis C 2010 Selective Hydrogenation of 1,3-Butadiene in the Presence of an Excess of Alkenes over Supported Bimetallic Gold−Palladium Catalysts *J. Phys. Chem. C* **114** 10823–35

[15] Cooper A, Bachiller-Baeza B, Anderson J A, Rodriguez-Ramos I and Guerrero-Ruiz A 2014 Design of surface sites for the selective hydrogenation of 1,3-butadiene on Pd nanoparticles: Cu bimetallic formation and sulfur poisoning *Catal. Sci. Technol.* **4** 1446–55

[16] Studt F, Abild-Pedersen F, Bligaard T, Sorensen R Z, Christensen C H and Nørskov J K 2008 Identification of Non-Precious Metal Alloy Catalysts for Selective Hydrogenation of Acetylene *Science* **320** 1320–2

[17] Sachtler W M H 1976 Chemisorption Complexes on Alloy Surfaces *Catal. Rev. Sci. Eng.* **14** 193–210

[18] Borodziński A and Bond G C 2008 Selective Hydrogenation of Ethyne in Ethene-Rich Streams on Palladium Catalysts, Part 2: Steady-State Kinetics and Effects of Palladium Particle Size, Carbon Monoxide, and Promoters *Catal. Rev. Sci. Eng.* **50** 379–469

[19] Armbrüster M, Kovnir K, Friedrich M, Teschner D, Wowsnick G, Hahne M, Gille P, Szentmiklósi L, Feuerbacher M, Heggen M, Girgsdies F, Rosenthal D, Schlögl R and Grin Y 2012 $Al_{13}Fe_4$ as a low-cost alternative for palladium in heterogeneous hydrogenation *Nat. Mater.* **11** 690–3

[20] Armbrüster M, Kovnir K, Grin J, Schlögl R, Gille P, Heggen M and Feuerbacher M 2012 Ordered cobalt-aluminum and iron-aluminum intermetallic compounds as hydrogenation catalysts. US Patent 20120029254

[21] Piccolo L 2013 $Al_{13}Fe_4$ selectively catalyzes the hydrogenation of butadiene at room temperature *Chem. Commun.* **49** 9149–51

[22] Piccolo L and Kibis L 2015 The partial hydrogenation of butadiene over $Al_{13}Fe_4$: A surface-science study of reaction and deactivation mechanisms *J. Catal.* **332** 112–8

[23] Piccolo L, Kibis L, De Weerd M-C, Gaudry E, Ledieu J and Fournée V 2017 Intermetallic Compounds as Potential Alternatives to Noble Metals in Heterogeneous Catalysis: The Partial Hydrogenation of Butadiene on γ-Al_4Cu_9(1 1 0) *ChemCatChem* **9** 2292–6

[24] Meier M, Ledieu J, Fournée V and Gaudry É 2017 Semihydrogenation of Acetylene on Al_5Co_2 Surfaces *J. Phys. Chem. C* **121** 4958–69

[25] Kandaskalov D, Fournée V, Ledieu J and Gaudry É 2014 Adsorption Properties of the o-$Al_{13}Co_4$(100) Surface toward Molecules Involved in the Semihydrogenation of Acetylene *J. Phys. Chem. C* **118** 23032–41

[26] Kandaskalov D, Fournée V, Ledieu J and Gaudry É 2017 Catalytic Semihydrogenation of Acetylene on the (100) Surface of the o-$Al_{13}Co_4$ Quasicrystalline Approximant: Density Functional Theory Study *J. Phys. Chem. C* **121** 18738–45

[27] Lin Q and Miller G J 2018 Electron-Poor Polar Intermetallics: Complex Structures, Novel Clusters, and Intriguing Bonding with Pronounced Electron Delocalization *Acc. Chem. Res.* **51** 49–58

[28] Ledieu J, Gaudry É and Fournée V 2014 Surfaces of Al-based complex metallic alloys: atomic structure, thin film growth and reactivity *Sci. Technol. Adv. Mater.* **15** 034802

[29] Dolinšek J, Komelj M, Jeglič P, Vrtnik S, Stanić D, Popčević P, Ivkov J, Smontara A, Jagličić Z, Gille P and Grin Y 2009 Anisotropic magnetic and transport properties of orthorhombic $Al_{13}Co_4$ *Phys. Rev. B* **79** 184201

[30] Popčević P, Smontara A, Ivkov J, Wencka M, Komelj M, Jeglič P, Vrtnik S, Bobnar M, Jagličić Z, Bauer B, Gille P, Borrmann H, Burkhardt U, Grin Y and Dolinšek J 2010 Anisotropic physical properties of the $Al_{13}Fe_4$ complex intermetallic and its ternary derivative $Al_{13}(Fe,Ni)_4$ *Phys. Rev. B* **81** 184203

[31] Smontara A, Popčević P, Stanić D, Velebit K and Dolinšek J 2011 Anisotropic transport properties of the $Al_{13}TM_4$ and T-Al–Mn–Fe complex metallic alloys *Philos. Mag.* **91** 2746–55

[32] Krajčí M and Hafner J 2011 Complex intermetallic compounds as selective hydrogenation catalysts – A case study for the (100) surface of $Al_{13}Co_4$ *J. Catal.* **278** 200–7

[33] Yamada T, Kojima T, Abe E, Kameoka S, Murakami Y, Gille P and Tsai A P 2018 Probing Single Pt Atoms in Complex Intermetallic $Al_{13}Fe_4$ *J. Am. Chem. Soc.* **140** 3838–41

[34] Schimpf S, Gaube J and Claus P 2004 Selective Hydrogenation of Multiple Unsaturated Compounds *Basic Principles in Applied Catalysis* Springer Series in Chemical Physics ed P D M Baerns (Springer Berlin Heidelberg) pp 85–123

[35] Bond G C, Webb G, Wells P B and Winterbottom J M 1965 587. The hydrogenation of alkadienes. Part I. The hydrogenation of buta-1,3-diene catalysed by the Noble Group VIII metals *J. Chem. Soc.* 3218–27

[36] Boitiaux J P, Cosyns J and Vasudevan S 1983 Hydrogenation of highly unsaturated hydrocarbons over highly dispersed palladium catalyst: Part I: behaviour of small metal particles *Appl. Catal.* **6** 41–51

[37] Piccolo L, Valcarcel A, Bausach M, Thomazeau C, Uzio D and Berhault G 2008 Tuning the shape of nanoparticles to control their catalytic properties: selective hydrogenation of 1,3-butadiene on Pd/Al2O3 *Phys. Chem. Chem. Phys.* **10** 5504–6

[38] Phillipson J J, Wells P B and Wilson G R 1969 The hydrogenation of alkadienes. Part III. The hydrogenation of buta-1,3-diene catalysed by iron, cobalt, nickel, and copper *J. Chem. Soc. A* 1351–63

[39] Moyes R B, Wells P B, Grant J and Salman N Y 2002 Electronic effects in butadiene hydrogenation catalysed by the transition metals *Appl. Catal. A* **229** 251–9

[40] Ledieu J, Gaudry É, Pussi K, Jarrin T, Scheid P, Gille P and Fournée V 2017 Reconstruction of the $Al_{13}Ru_4$ (010) Approximant Surface Leading to Anisotropic Molecular Adsorption *J. Phys. Chem. C* **121** 22067–72

[41] Shin H, Pussi K, Gaudry É, Ledieu J, Fournée V, Alarcón Villaseca S, Dubois J-M, Grin Y, Gille P, Moritz W and Diehl R D 2011 Structure of the orthorhombic $Al_{13}Co_4$(100) surface using LEED, STM, and ab initio studies *Phys. Rev. B* **84** 085411

[42] Gaudry É, Chatelier C, McGuirk G M, Serkovic Loli L N, de Weerd M-C, Ledieu J, Fournée V, Felici R, Drnec J, Beutier G and de Boissieu M 2016 Structure of the $Al_{13}Co_4$ surface: Combination of surface x-ray diffraction and ab initio calculations *Phys. Rev. B* **94** 165406

[43] Ledieu J, Gaudry E, Loli L N S, Villaseca S A, de Weerd M-C, Hahne M, Gille P, Grin Y, Dubois J-M and Fournée V 2013 Structural Investigation of the (010) Surface of the $Al_{13}Fe_4$ Catalyst *Phys. Rev. Lett.* **110** 076102

[44] Gille P and Bauer B 2008 Single crystal growth of $Al_{13}Co_4$ and $Al_{13}Fe_4$ from Al-rich solutions by the Czochralski method *Cryst. Res. Technol.* **43** 1161–7

[45] Morfin F and Piccolo L 2013 A versatile elevated-pressure reactor combined with an ultrahigh vacuum surface setup for efficient testing of model and powder catalysts under clean gas-phase conditions *Rev. Sci. Instrum.* **84** 094101

[46] Grin J, Burkhardt U, Ellner M and Peters K 1994 Crystal structure of orthorhombic Co_4Al_{13} *J. Alloys Compd.* **206** 243–7

[47] Grin J, Burkhardt U, Ellner M and Peters K 1994 Refinement of the Fe_4Al_{13} structure and its relationship to the quasihomological homeotypical structures *Z. Kristallogr.* **209** 479–87

[48] Murao R, Genba M, Sugiyama K and Sun W 2011 The Structure of an Al-Ni-Ru Monoclinic Phase $Al_{13}(Ru,Ni)_4$ *Mater. Trans.* **52** 1344–8

[49] Edshammar L-E, Nyberg B and Vänngård T 1965 The Crystal Structure of Ru_4Al_{13} *Acta Chem. Scand.* **19** 2124–30

[50] Henley C L 2006 Clusters, phason elasticity and entropic stabilization: a theoretical perspective *Philos. Mag.* **86** 1123–9

[51] Scheid P, Chatelier C, Ledieu J, Fournée V and Gaudry É 2019 Bonding network and stability of clusters: the case study of Al13TM4 pseudo-tenfold surfaces *Acta Cryst A* **75** 314–24

[52] Kresse G and Furthmüller J 1996 Efficiency of ab-initio total energy calculations for metals and semiconductors using a plane-wave basis set *Comput. Mater. Sci.* **6** 15–50

[53] Kresse G and Furthmüller J 1996 Efficient iterative schemes for ab initio total-energy calculations using a plane-wave basis set *Phys. Rev. B* **54** 11169–86

[54] Kresse G and Hafner J 1993 Ab initio molecular dynamics for liquid metals *Phys. Rev. B* **47** 558–61

[55] Kresse G and Hafner J 1994 Ab initio molecular-dynamics simulation of the liquid-metal–amorphous-semiconductor transition in germanium *Phys. Rev. B* **49** 14251–69

[56] Kresse G and Joubert D 1999 From ultrasoft pseudopotentials to the projector augmented-wave method *Phys. Rev. B* **59** 1758–75

[57] Blöchl P E 1994 Projector augmented-wave method *Phys. Rev. B* **50** 17953–79

[58] Perdew J P, Burke K and Ernzerhof M 1996 Generalized gradient approximation made simple *Phys. Rev. Lett.* **77** 3865–8

[59] Perdew J P, Burke K and Ernzerhof M 1997 Generalized Gradient Approximation Made Simple [Phys. Rev. Lett. 77, 3865 (1996)] *Phys. Rev. Lett.* **78** 1396–1396

[60] Grimme S, Ehrlich S and Goerigk L 2011 Effect of the damping function in dispersion corrected density functional theory *J. Comput. Chem.* **32** 1456–65

[61] Mihalkovič M and Widom M 2007 First-principles calculations of cohesive energies in the Al-Co binary alloy system *Phys. Rev. B* **75** 014207

[62] Momma K and Izumi F 2011 VESTA 3 for three-dimensional visualization of crystal, volumetric and morphology data *J. Appl. Cryst.* **44** 1272–6

[63] van Helden P, van den Berg J-A and Weststrate C J 2012 Hydrogen Adsorption on Co Surfaces: A Density Functional Theory and Temperature Programmed Desorption Study *ACS Catal.* **2** 1097–107

[64] Ciobica I M, Kleyn A W and Van Santen R A 2003 Adsorption and Coadsorption of CO and H on Ruthenium Surfaces *J. Phys. Chem. B* **107** 164–72

[65] Kristinsdóttir L and Skúlason E 2012 A systematic DFT study of hydrogen diffusion on transition metal surfaces *Surf. Sci.* **606** 1400–4

[66] Kitchin J R, Nørskov J K, Barteau M A and Chen J G 2004 Role of Strain and Ligand Effects in the Modification of the Electronic and Chemical Properties of Bimetallic Surfaces *Phys. Rev. Lett.* **93** 156801-1–4

[67] Mavrikakis M, Hammer B and Nørskov J K 1998 Effect of Strain on the Reactivity of Metal Surfaces *Phys. Rev. Lett.* **81** 2819–22

[68] Vojvodic A, Nørskov J K and Abild-Pedersen F 2014 Electronic Structure Effects in Transition Metal Surface Chemistry *Top. Catal.* **57** 25–32

[69] Nørskov J K, Studt F, Abild-Pedersen F and Bligaard T 2014 *Fundamental Concepts in Heterogeneous Catalysis* (Hoboken, New Jersey: Wiley)

[70] Greiner M T, Jones T E, Beeg S, Zwiener L, Scherzer M, Girgsdies F, Piccinin S, Armbrüster M, Knop-Gericke A and Schlögl R 2018 Free-atom-like d states in single-atom alloy catalysts *Nat. Chem.* **10** 1008–15

[71] Loffreda D, Michel C, Delbecq F and Sautet P 2013 Tuning catalytic reactivity on metal surfaces: Insights from DFT *J. Catal.* **308** 374–85